

Charge Pump Detector: Optimization with Process and Device Simulation

Julie D. Segal and Christopher J. Kenney

SLAC National Accelerator Laboratory, 2575 Sand Hill Road, Menlo Park, CA 94025 USA

Abstract—The charge pump pixel detector concept was developed to meet the requirements of x-ray correlation spectroscopy. The sensor is built in high resistivity silicon with front and backside diffused regions and double metal processing on the front side. The design is targeted for low noise of less than 100 electrons, high quantum efficiency for 8KeV photons, 8mS readout for the entire array, and dynamic range of 100 photons. The pixel size is 56 μ m by 56 μ m. In the current work, extensive TCAD simulations were used to optimize the device structure, the bias conditions, and the process conditions. 3D simulations under dynamic switching conditions were executed to study charge cloud evolution, charge storage, and read-out.

I. INTRODUCTION

The charge-pump pixel detector concept was first proposed by Pavel Rehak [1]. The device operation is similar to the pn-ccd, where signal charge is stored in a potential well controlled by a reverse-biased diode and then passed to the read-out node. In the charge pump pixel detector, the charge is not passed down the column but instead read-out to the column line directly from each pixel under the control of the row-lines. The design is targeted to meet the requirements of X-ray Correlation Spectroscopy: low noise of less than 100 electrons, high quantum efficiency for 8KeV photons, 8mS readout for the entire array, and dynamic range of 100 photons.

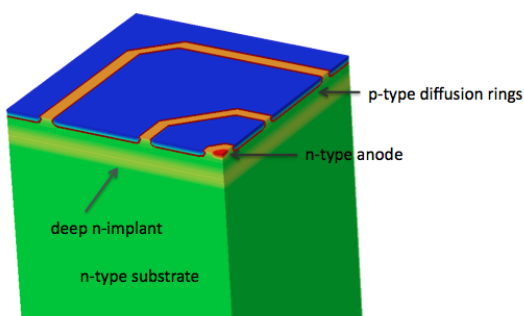


Figure 1: Illustration of key features of pixel cell structure. $\frac{1}{4}$ of a single pixel is shown. Full pixel dimensions are 56 μ m x 56 μ m from the top view, and 300 μ m deep. The substrate is high resistivity n-type silicon. Three p-type rings surround an n-type anode. A deep n-type implant is located approximately 3.2 μ m from the front surface.

The original design was targeted for fabrication at BNL [1]. In the current work, the process and device design are targeted for fabrication at SNF (Stanford Nanofabrication Facility).

(email jsegal@slac.stanford.edu).

II. STRUCTURE AND OPERATION

The charge pump pixel structure is illustrated in Fig 1. The starting material is 300 μ m thick high-resistivity n-type silicon. The pixel size is 56 μ m by 56 μ m. There are three p-type diffusion rings surrounding an n+ anode in the center of the pixel. The p-type rings are biased dynamically to control the collection and read-out of the charge. A deep n-type blanket implant, about 3.2 μ m from the surface, determines the location of the potential well for collecting and storing electrons until the read-out.

The backside of the device (not shown) has an implanted p-type diode, which is reverse-biased to fully deplete the bulk during operation. The backside also serves as the entrance window for x-rays.

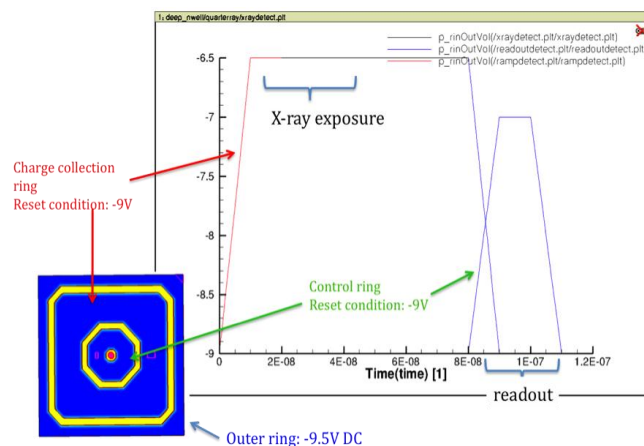


Figure 2: Detector Bias Conditions used for simulations. The n+ anode is biased at 0V, and the three p+ rings are biased as shown. The charge is collected under middle p+ ring, and the read-out gated by the inner control ring. The outer p+ rings is kept at a constant voltage chosen to help bias the signal electrons towards the center of the pixel.

The n+ anode is connected directly to the column line, routed in second layer metal. The two inner p+ rings are controlled with row lines routed in first layer metal. Figure 2 shows the operation and biasing of the pixel. The anode is biased at 0V, the backside p+ diode is biased at -90V for 300 μ m thick silicon, and the p+ rings are biased as shown in the figure. The charge (electrons) generated from the x-ray absorption are collected and stored under the middle ring, or charge collection ring. The inner ring, or control ring, is used to control the read-out at the end of the collection period. The

outer ring is DC-bias to create a drift field for electrons toward the center of the pixel.

III. DEVICE SIMULATION

The charge pump pixel device structure was designed using Synopsys TCAD Sentaurus device simulations. Simulation of the electrostatic potential can be performed on $\frac{1}{4}$ pixel, due to the symmetry of the pixel. Certain simulations of charge cloud evolution and charge collection were performed on a full pixel. Fig. 3 shows simulated electrostatic potential for an optimized design. The bias conditions for the simulation are shown in Fig. 2. In Fig. 3a, the pixel is in stand-by mode, with all three rings reversed-biased at a similar potential. For x-ray exposure and charge collection, the middle ring, or collection ring, is biased positively compared to the other rings under dynamic conditions to create a potential well for electrons. The resulting potential distribution is shown in Fig. 3b, where potential well for electrons can be seen under the middle p-ring. Note that this potential well can only be accurately simulated under dynamic simulation conditions. Under equilibrium conditions, or DC simulations, electrons created by electron/hole pair generation fill the potential well.

Because 2D simulations are far less computationally intensive, we use 2D cross sections wherever possible. However, when we compared 2D device simulation results to 3D device simulation results we found that 2D simulations have very limited usefulness for this structure. The radial nature of the pixel geometry strongly effects the potential distribution, with the rings exerting strong inward effects.

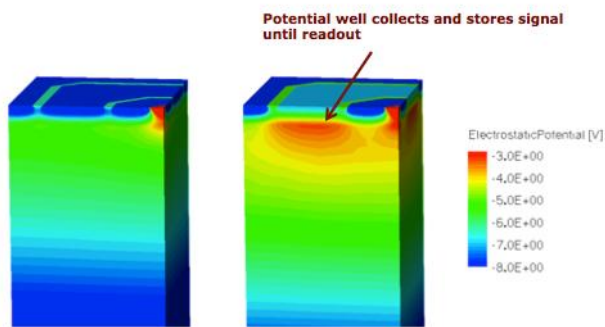


Figure 3: AC Device simulation of $\frac{1}{4}$ pixel showing *electrostatic potential*. Referring to timing shown in Fig. 2: (a) at time= 0, or stand-by condition, and (b) at time = $2E-8$ seconds, when the pixel is biased to collect and store electrons. Note the potential well for electrons under the middle p-ring.

The evolution of the electron cloud generated by x-ray absorption is simulated in Fig. 4. In Fig. 4a the electron cloud drifts toward the surface of the pixel. Fig. 4b and Fig. 4c show the collection stage and the read-out stage respectively.

Dynamic device simulations were executed to verify that the design meets the application requirements for full well capacity. Fig. 5 shows the simulated anode current during the read-out phase of the detector operation. Complete charge read-out is achieved for the charge equivalent of up to 100 8KeV photons, assuming 2200 electron/hole pairs generated

per photon. Note that charge sharing is not simulated, so in practice some of the charge might diffuse to adjacent pixels, depending on the signal intensity in those pixels.

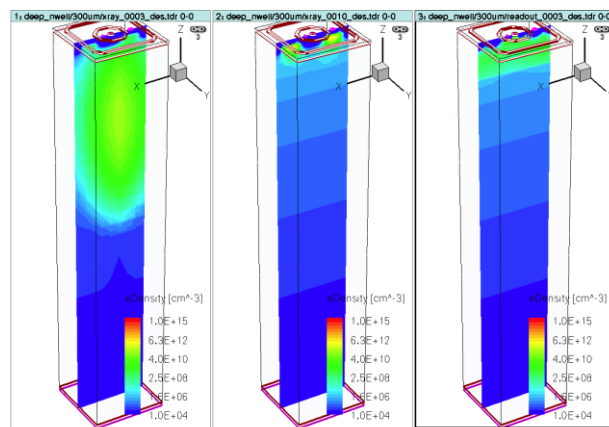


Figure 4: AC device simulation of full pixel showing charge cloud evolution and read-out. *Electron density* is shown at (a) 5ns and (b) 50ns after the x-ray is absorbed. The final figure (c) shows the read-out phase.

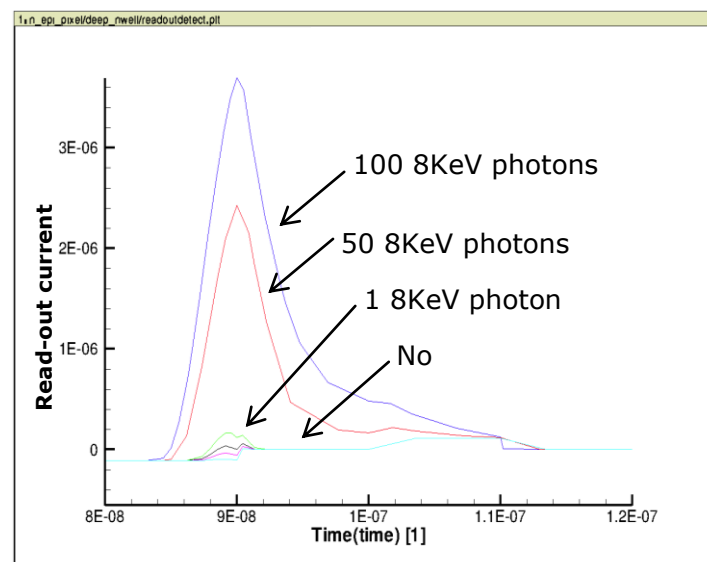


Figure 5: Simulated anode current during the read-out phase of pixel operation. Read-out signal is linear up to the full well capacity requirement of 100 8 keV photons

Verification of the target device only is not adequate to ensure success. Inevitably, process variations will occur and the target design will not be perfectly realized. Therefore, part of the device optimization involves simulating the likely process variations and verifying the correct behavior. The design is then re-targeted for the center of the range of process variations with functional results. Process variations that were simulated include ring width and space, junction depth, deep n-implant depth. P-type rings are implanted through field oxide openings, so ring width and space is controlled by field oxide mask and etch. These parameters are expected to be most subject to variation since lithography bias and etch bias

are difficult to predict. If the rings are too close together, or the surface implant is too high, punch-thru current between the p-rings results. But if the rings are too far apart, the potential well is not isolated from the oxide-silicon surface between rings, and generated carriers from this region prevent the formation of an adequate collection well.

High electric field regions in silicon diodes can lead to avalanche breakdown. There are two possible high field areas in the charge pump pixel detector: the diode between the anode and inner p-ring, and the backside high voltage diode termination. These regions were studied to insure the peak electric field is well below the breakdown voltage and to optimize the floating ring layout around the backside diode.

Finally, simulations were also used to determine optimum applied voltage conditions, and the robustness of the design to voltage variations.

IV. PROCESS

Synopsys Sentaurus TCAD Process simulations were used to design a process flow that would result in the target device structure designed based on the device simulation results. The parameters optimized with process simulations include implant doses and energies, dopant drive-in and activation time and temperatures, and oxidation conditions. These steps are interdependent so the full process must be simulated. Process simulation results are shown for key features of the structure in Fig. 6.

A schematic view of the final cross section is shown in Fig. 7. There are 11 masking steps, including 3 backside-masking steps. 8 masking steps are performed on an ASML stepper. 4 masking steps, including the three backside steps and the pad opening on the front side, use whole-wafer contact align, making this a “mix-and-match” mask set. The frontside has four implant steps: deep phosphorus implant and a surface arsenic implant are blanket implants, phosphorus anode and boron rings are masked. The process has two levels of metal interconnect on the frontside. The backside has one masked implant and one metal layer.

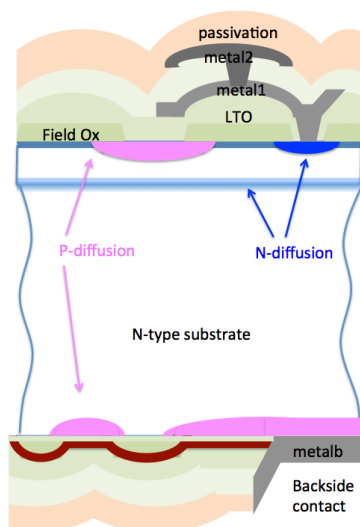


Figure 7: Illustration (not to scale) of final process cross section. The process has 8 topside masks and 3 backside masks

V. MASK LAYOUT

Design parameters such as front-side ring width and spacing and backside floating ring design are determined from simulations. Based on these results the mask layout is implemented. Certain results from process simulations, such as side diffusion of masked implants, must also be considered. A portion of the sensor layout is shown in Fig. 8.

VI. CONCLUSION

Extensive TCAD simulations were used to optimize the device structure, the bias conditions, and the process conditions of the charge pump pixel detector. We executed full 3D simulations of the pixel under dynamic switching conditions to understand the charge cloud evolution, charge storage, and read-out.

At the time of this writing, the detectors have been processed and are under test.

REFERENCES

- [1] G. A. Carini, P. Rehak, W. Chen, D. P. Siddons, “ Charge-pump detector for X-ray correlation spectroscopy”, *Nucl. Instrum. and Methods*, A649, pp. 75-77, 2011.

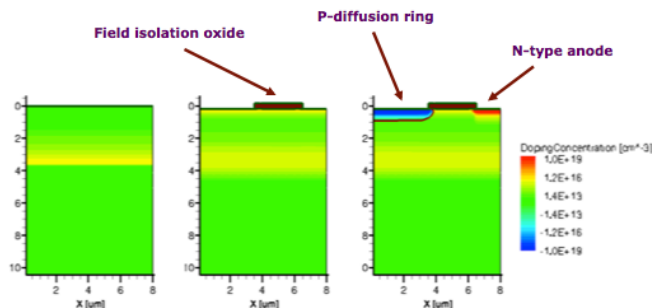


Figure 6: Process simulation results shown after (a) deep n-implant, (b) surface implant, field oxidation, and field oxide mask/etch, and (c) n-anode and p-rings.

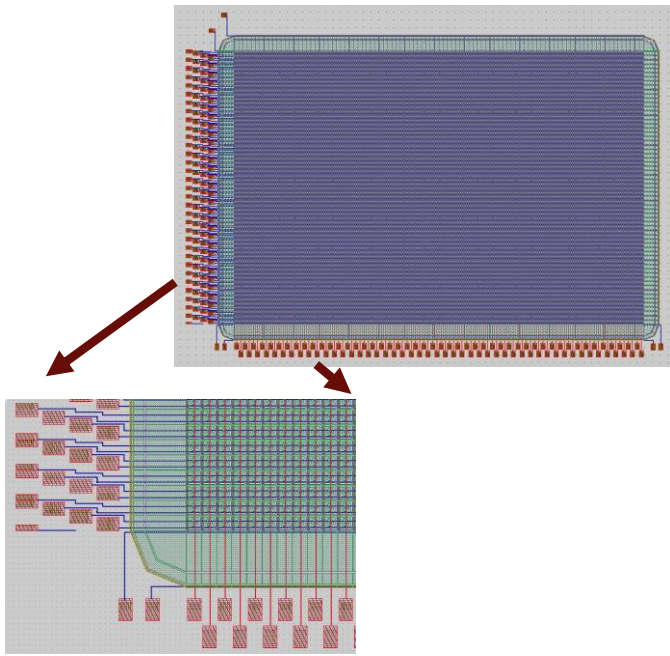


Figure 8: Mask Design Layout of small (96 X 64) pixel detector. Blue is first layer metal, red is second layer metal, green is p-type diffusion, yellow is n-type diffusion.